Standing waves, clustering, and phase–waves in 1d-simulations of kinetic relaxation oscillations in NO+NH_3 on Pt(100) coupled by diffusion

October 10, 2003

Hannes Uecker

Mathematisches Institut I, Universität Karlsruhe,

hannes.uecker@math.uni-karlsruhe.de

Abstract

The Lombardo–Imbihl–Fink (LFI) ODE model of the NO+NH_3 reaction on a Pt(100) surface shows stable relaxation oscillations with very sharp transitions for temperatures T between 404K and 433K. Here we study numerically the effect of linear diffusive coupling of these oscillators in one spatial dimension. Depending on the parameters and initial conditions we find a rich variety of spatio–temporal patterns which we group into 4 main regimes: bulk oscillations (BO), standing waves (SW), phase clusters (PC), and phase waves (PW). Two key ingredients for SW and PC are identified, namely the relaxation type of the ODE oscillations and a nonlocal (and nonglobal) coupling due to relatively fast diffusion of the kinetically slaved variables NH_3 and H. In particular, the latter replaces the global coupling through the gas phase used to obtain SW and PC in models of related surface reactions. The phase waves exist only under the assumption of (relatively) slow diffusion of NH_3 and H.

1 Introduction

Because of the deleterious effects of substances like NO in the atmosphere it is desirable to reduce these substances. In [24] the catalytic reduction of NO with NH_3 to the products N_2 and H_2O has been studied experimentally on a Pt(100) surface. This surface can switch between two substrate configurations, a catalytically active 1×1 phase with a bulk–like surface termination and a quasi–hexagonal reconstructed phase ("hex") which is catalytically inert. The stable state of the clean Pt(100) surface is the hex reconstruction but above a critical adsorbate coverage the 1×1 phase is more stable and the reconstruction is lifted. Thus an adsorbate-induced 1×1↔ hex phase transition is constituted. In [14] a model for this reaction has been set up. Neglecting reaction intermediates like NH and NH_2 one arrives at a 7–dimensional system of ordinary differential equations (ODE) for $\theta_{\rm NO}^{1\times1}, \theta_{\rm NO}^{\rm hex}, \theta_{1\times1}, \theta_{\rm NH_3}^{1\times1}, \theta_{\rm O}^{1\times1}, \theta_{\rm N}^{1\times1}, \theta_{\rm H}^{1\times1}$, which correspond to, in that order, the local coverages of NO on the 1×1–phase, of NO on the hex–phase, the fraction $\theta_{1\times1}$ of the surface in 1×1–phase, and to the local coverages of NH_3, O, N and H on the 1×1–phase. We write the ODE in abstract form as

$$\frac{\rm d}{{\rm d}t}X = f(X;p,T), \quad X \in \mathbb{R}^7, \quad f = (f_1,\dots,f_7), \tag{1.1}$$

where $p \in \mathbb{R}^{11}$ is a vector of (fixed) temperature independent parameters. Moreover, (1.1) contains 11 rate constants depending by Arrhenius-law on temperature T, which we therefore

display explicitly. In p there are two external (tunable) parameters, $\mathrm{p_{NO}}$, and $\mathrm{p_{NH_3}}$, acting as driving forces and corresponding to a constant supply of NO and NH_3, respectively, from the gas phase.

Similar to experimental data, the model shows oscillations in a temperature range from 404K to 433K. However, the oscillations in the model are strongly of relaxation type while in the experiment they appear to be much more harmonic. In section 2 we plot typical periodic orbits of (1.1), but we will not repeat in detail the properties of this ODE; see App.A for the equations, and [14, 23] for discussion and detailed numerical analysis of (1.1). Here we study numerically the effect of linear diffusive coupling of the ODE oscillators in one dimension, i.e., we consider

$$\frac{\mathrm{d}}{\mathrm{d}t}X(t,x) = f(X(t,x);p,T) + M(T)\nabla^2 X(t,x), \tag{1.2}$$

where $M(T)$ is the diagonal diffusion matrix depending on T. Depending on the parameters, i.e., T and the diffusion constants $D_{\mathrm{NO}}^{1\times1}, D_{\mathrm{NO}}^{\mathrm{hex}}, D_{\mathrm{NH_3}}, D_{\mathrm{H}}$ (O and N are immobile in the temperature ranges considered here and hence $D_{\mathrm{O}} = D_{\mathrm{N}} = 0$), we find 4 different regimes: bulk oscillations (BO), standing waves (SW), phase clusters (PC), and phase–waves (PW).

Here BO means that the whole surface oscillates homogeneously in the limit cycle of (1.2), while in both SW and PC the oscillations are organized into macroscopic areas of roughly equal size in such a way that the phase changes from one area to the next in a regular way, with phase shifts of half a period. Such macroscopic areas of equal phase will be called clusters in the following. The difference between SW and PC is that in SW the phase–pattern has an intrinsic spatial wave–length, while in PC the clusters have no intrinsic size and grow until the whole domain is split into only 2 clusters. Here we follow [1, 18, 8, 3] in the terminology, while sometimes both SW and PC are just called clustering. Both SW and PC require substantial deviations from the periodic ODE orbits in particular at the cluster boundaries, while in PW the phase changes smoothly and each individual oscillator is always close to the periodic ODE orbit.

Due to the large number of parameters in the problem, the transitions between the different regimes are rather delicate. The system is most sensitive with respect to the (relatively small) NO diffusions on the 1×1 and the hex phase, respectively. This agrees well with the analysis in [23] where it is shown that $\theta_{\mathrm{NO}}^{1\times1}, \theta_{\mathrm{NO}}^{\mathrm{hex}}$ and $\theta_{1\times1}$ are the important dynamic variables for (1.1) (in the oscillatory regime) while the remaining four are slaved. However, $\theta_{1\times1}$ does not diffuse, which gives NO–diffusion its special importance.

One effect of SW and PC is that both reduce the periods of oscillations of macroscopic (i.e. spatially averaged) quantities by a factor of roughly 2. This might explain a mismatch in periods [14, fig.7] between the experimentally observed oscillations and the numerical simulations of (1.1). Moreover, while (1.1) has relaxation oscillations with very sharp transitions, the averaged quantities oscillate more harmonically which also fits much better to the experimental data.

Of course, BO, SW, PC and PW (and the competition between these patterns) are also very interesting from a theoretical point of view. Phase waves (and phase turbulence) for oscillators close to a Hopf point are usually analyzed using phase diffusion equations; see [12, section 4] for an introduction. However, relaxation oscillators may behave quite differently under (weak) coupling than harmonic oscillators [22, 9]. This theory has been mainly developed using models related to neurobiology. In particular, for certain classes of weakly coupled relaxation oscillators there are no PW solutions, while BO, SW and PC may be exponentially stable [9]. In contrast, stationary solutions of diffusion equations (on large domains) are at best diffusively stable [15], i.e., perturbations decay with an algebraic rate. Yet the theoretical understanding of SW and PC is still quite limited. Additional to [22, 9] see [16, section 5] and the references therein for a description of clustering (and chaos) in chains and circles of bistable oscillators, containing some analytical results.

In chemistry, SW and PC have been intensively studied for the CO oxidation on Pt(110), both experimentally and theoretically [1, 7, 8, 19, 18, 3, 5, 4]. Here the reaction–diffusion models have considerably simpler (3 dimensional or, in a refined version, 4 dimensional) ODE dynamics than (1.1), but additional to the surface diffusion there is a *global* coupling through the gas phase in the spatially extended system. Moreover, external forcing [18] and/or global delayed feedback [10, 3, 5, 4] have been used to *control* the pattern formation in this system. Similarly, in [25] a global feedback has been used to obtain clustering in a reaction–diffusion model of the Belousov–Zhabotinsky reaction with 2 dimensional kinetics.

In [23] we show that the ODE (1.1) can also be reduced to a 3 dimensional system

$$\frac{\mathrm{d}}{\mathrm{d}t}y = g(y;p,T), \quad y = \begin{pmatrix} \theta_{\mathrm{NO}}^{1\times1} \\ \theta_{\mathrm{NO}}^{\mathrm{hex}} \\ \theta_{1\times1} \end{pmatrix}, \quad g(y) = \begin{pmatrix} f_1(\theta_{\mathrm{NO}}^{1\times1}, \theta_{\mathrm{NO}}^{\mathrm{hex}}, \theta_{1\times1}, h(y)) \\ f_2(\theta_{\mathrm{NO}}^{1\times1}, \theta_{\mathrm{NO}}^{\mathrm{hex}}, \theta_{1\times1}, h(y)) \\ f_3(\theta_{\mathrm{NO}}^{1\times1}, \theta_{\mathrm{NO}}^{\mathrm{hex}}, \theta_{1\times1}, h(y)) \end{pmatrix} \tag{1.3}$$

for the slow variables y by adiabatic elimination of the fast variables $z{=}(\theta_{\mathrm{NH_3}}^{1\times1}, \theta_{\mathrm{O}}^{1\times1}, \theta_{\mathrm{N}}^{1\times1}, \theta_{\mathrm{H}}^{1\times1})$. Chemically, the key role of NO is due to the fact that in (1.1) the lifting of the hex reconstruction proceeds through NO adsorption, i.e., NO induces the hex$\to$ 1×1 phase transition. Naively, we may then study the reaction diffusion problem

$$\frac{\mathrm{d}}{\mathrm{d}t}y = g(y;p,T) + M_{\mathrm{red}}\nabla^2 y, \quad M_{\mathrm{red}} = \mathrm{diag}(D_{\mathrm{NO}}^{1\times1}, D_{\mathrm{NO}}^{\mathrm{hex}}, 0). \tag{1.4}$$

However, although the error between (1.1) and (1.3) is very small, obviously all the influence of the (relatively fast) diffusion of NH_3 and H is lost in going from (1.2) to (1.4), which corresponds to (1.2) in the limit $D_{\mathrm{NH_3}}, D_{\mathrm{H}} = 0$. Here we find that SW or PC do not occur in this limit or even for relatively slow diffusion of NH_3 and H, and, moreover, that *only* for slow or vanishing diffusion of NH_3 and H we find PW. This shows that, additional to the relaxation type of the oscillations, a key ingredient for SW and PC in (1.2) is a *nonlocal* (and nonglobal) coupling due to the relatively fast diffusion of the kinetically slaved variables $\theta_{\mathrm{NH_3}}^{1\times1}$ and $\theta_{\mathrm{H}}^{1\times1}$.

In sec.2 we show typical periodic orbits for (1.1) and in sec.3 we review results about weak coupling of relaxation vs. harmonic oscillators. Section 4 contains preparatory remarks about the diffusion constants, the numerical method and the choice of initial conditions for (1.2). In sections 5 and 6 we present our main results. Conclusions and open questions are given in sec.7. In App.A we present the ODE (1.1), and in App.B, related to (1.3), we comment on adiabatic reduction in (1.2).

2 The periodic ODE–orbits

Figure 1 shows periodic orbits for (1.1) at temperatures T=410, 420, 430 K. The partial pressures are $p_{NO} = 1.1\times10^{-6}$ mbar and $p_{NH_3} = 4.7\times10^{-6}$ mbar, as in [14]. The tem-

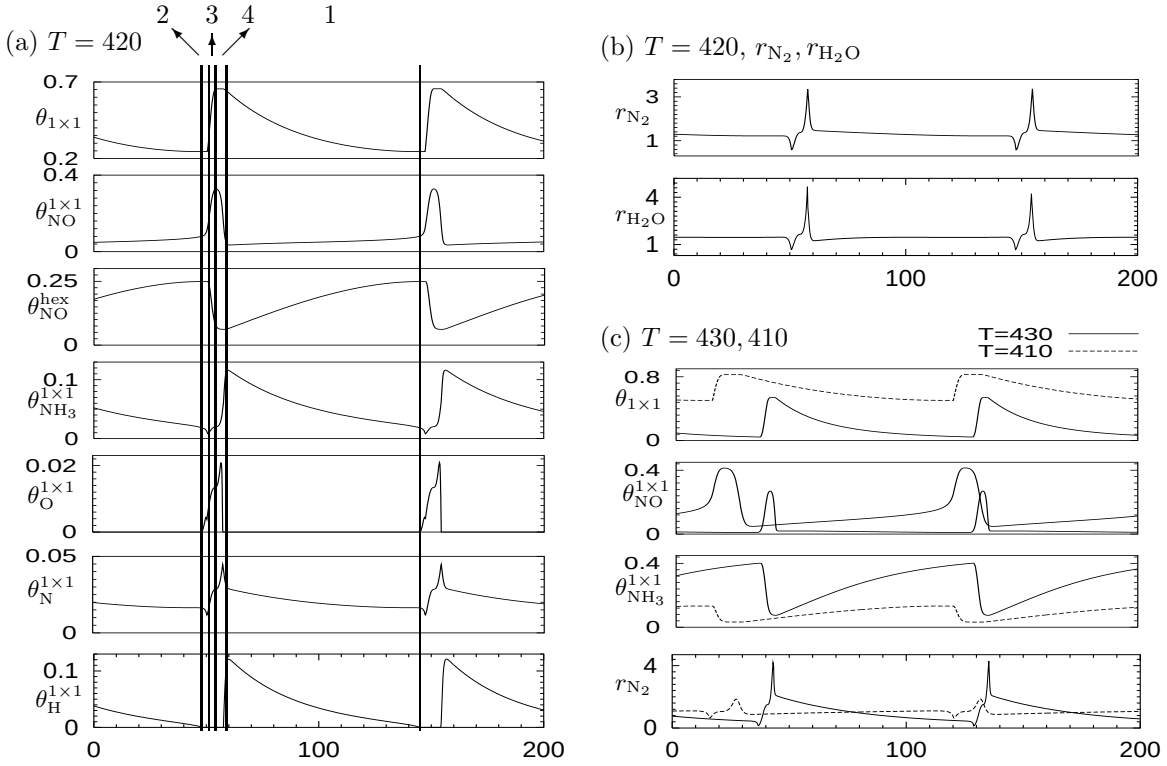

Figure 1: (a) periodic ODE–orbits at $T = 420$K, (b) production rates at $T = 420$K, (c) $\theta^{1\times1}_{NO}, \theta^{hex}_{NO}, \theta_{1\times1}, r_{N_2}$ at $T = 410, 430$K; time in s, coverages are dimensionless, production rates r_{N_2}, r_{H_2O} in 10^{14}cm^{-2}s^{-1}.

peratures were chosen for no particular reason, except that they are well in the oscillatory regime (404K$\leq T \leq$ 433K) with stable relaxation oscillations. We will consider the reaction–diffusion problem most thoroughly at $T = 420$K and only briefly comment on lower and higher temperatures. Fig.1(a) shows all 7 dynamic variables, and (b) the chemically interesting production rates $r_{N_2} = 0.5N_s k_9(\theta^{1\times1}_N)^2/\theta_{1\times1}$ of N_2 and $r_{H_2O} = N_s k_8 \theta^{1\times1}_O \theta^{1\times1}_H/\theta_{1\times1}$ of H_2O, where $N_s = 1.3\times10^{15}$ cm^{-2} is the concentration of surface sites.

We repeat the most important conclusions from [14, 23]. As in [23] we divide a period into four segments. The reason why we plot $\theta_{1\times1}$ first is that the decay of $\theta_{1\times1}$ in segment 1 sets the slowest time scale in the largest segment; here all other variables follow $\theta_{1\times1}$ adiabatically. This breaks down in segment 2, where adsorbtion of NO starts the hex$\rightarrow$1×1 phase transformation in segment 3. In segment 4 the so called "surface explosion" occurs with a rapid production of N_2 and H_2O. This leads to the build–up of an $NH_{x,ad}/H_{ad}$ layer, which is unable to stabilize the 1×1 phase. This yields the slow relaxation to the hex phase in segment 1 again. The different roles of the variables during the different segments and the associated different time–scales are analyzed in more detail in [23].

In fig.1(c) we only plot $\theta_{1\times1}, \theta_{NO}^{1\times1}, \theta_{NO}^{hex}$ and r_{N_2}. Lowering the temperature from 420K to 410K has two main effect: the (average) fraction $\theta_{1\times1}$ of the 1×1 phase increases, while the amplitude of the oscillations and the reaction rates decrease. Increasing T to 430K has the opposite effect. The period also depends on T but only slightly in the middle of the oscillatory regime considered here. Below the lower threshold ($T \approx 404K$) for oscillations the surface is completely in the 1×1 phase ($\theta_{1\times1} = 1$), while above the upper threshold ($T \approx 433K$) it is in the hex phase ($\theta_{1\times1} = 0$). In both cases, the production rates r_{N_2} and r_{H_2O} are zero.

For (1.2) two observations from fig.1 turn out to be most important. First, the smaller amplitudes at lower temperatures yield smaller spatial gradients for oscillators with shifted phases. Second, the transitions become less sharp for lower T; see sec.6 and 7.

3 Weak coupling of relaxation vs. harmonic oscillators

Given an ODE $\frac{\mathrm{d}}{\mathrm{d}t}X = f(X)$, $X \in \mathbb{R}^d$, with an asymptotically stable periodic orbit γ with period α, we can associate a scalar quantity ϕ called phase and defined by $\frac{\mathrm{d}}{\mathrm{d}t}\phi = \omega = 2\pi/\alpha$ in such a (normalized) way that ϕ changes from 0 to 2π along one period of γ. Thus we may assign a phase ϕ_q to every point q on γ. Next, ϕ can be extended in a natural way to a neighborhood $U(\gamma) \subset \mathbb{R}^d$ of γ (a "tube" around γ) by the method of asymptotic phase (see, e.g., [12]): let $p \in U(\gamma) \setminus \gamma$, and let $q \in \gamma$ be the unique point such that $\|p(t) - q(t)\| \to 0$ as $t \to \infty$; then set $\phi_p = \phi_q$. The $(d-1)$–dimensional subsets (hypersurfaces) of $U(\gamma)$ consisting of points of equal phase are called isochrons.

Now let

$$\frac{\mathrm{d}}{\mathrm{d}t}X_i = f(X_i) + \varepsilon g(X_1, X_2), \quad i = 1, 2, \tag{3.1}$$

be a weakly coupled system of two such oscillators, where $0 < \varepsilon \ll 1$ is the coupling strength. Then we can introduce a slow time $\tau = \varepsilon t$ such that (3.1) can be reduced (averaged) to

$$\frac{\mathrm{d}}{\mathrm{d}\tau}\chi = H(\chi) + \mathcal{O}(\varepsilon), \tag{3.2}$$

where $\chi = \chi(\tau) = \phi_2(\tau) - \phi_1(\tau)$ is the phase difference in slow time and H is a 2π–periodic scalar function. Ignoring the $\mathcal{O}(\varepsilon)$ terms (i.e., setting $\varepsilon = 0$) in (3.2), each root χ^* of $H(\chi) = 0$

corresponds to an in–phase solution of (3.1), which is stable if $H'(\chi^*) < 0$. For harmonic oscillators, H is smooth and $H(0) = 0$ (and also $H(\pi) = 0$ but usually $H'(\pi) > 0$). This is the starting point of the derivation of the phase–diffusion equation [12, section4] in the limit of infinitely many diffusively coupled oscillators, where in this continuum limit the (linear) stability of BO can be evaluated from the associated dispersion relation.

Weakly coupled relaxation oscillators can behave fundamentally different. In particular, let $0 < \mu \ll 1$ be the ratio of the slow to the fast timescale(s) in the relaxation oscillation. Then the function H in (3.2) may become discontinuous in the limit $\mu \to 0$, with a negative jump at $\chi = 0$; see [9], where also explicit formulas for $\lim_{\mu\to 0} H$ are given. As a consequence, solutions $\chi = 0$ of (3.2) persist with a rapid convergence even for $\varepsilon > 0$. This implies that these in–phase solutions with $\chi = 0$ persist for (3.1), and moreover, that traveling phase–waves do not exist for the generalization of (3.1) to (certain) fields of relaxation oscillators [9, Cor.4.4]. Moreover, in [9], explicit formulas are given such that anti–phase solutions ($\chi^* = \pi$) are exponentially stable. These results hold in the singular limit $0 < \mu \ll \varepsilon \ll 1$. Similar results were obtained in [22] for $0 < \mu, \varepsilon \ll 1$ using the more geometric FTM (fast threshold modulation) theory; see also [11] and the references therein.

In the present paper, we will not explicitly apply these results to (1.2). However, the connection of the simulations of (1.2) to the theory above is striking: very rapid convergence to in–phase ($\chi = 0$) solutions (BO) or anti–phase ($\chi = \pi$) solutions (SW or PC). This is further discussed in sec.7.

4 Setup for the reaction–diffusion system

4.1 The diffusion constants

Surface diffusion constants are notoriously difficult to measure and the results of different experimental methods for the same system often vary over orders of magnitude; see [20, 2] for a review on the determination of diffusion constants from experiments and/or first principles. For Pt(100)/H,N,O,NO,NH_3 no diffusion data are available. Hence, here we approximate the diffusion constants of the various species using, as usual, the Arrhenius–law $D_i = \nu \mathrm{e}^{-\tilde{E}_i/RT}$, where $R = 8.3144$ J K^{-1}mol is the universal gas constant, $\nu = 0.001$ cm^{2}s^{-1} is a common prefactor, and where the activation energies for diffusion $\tilde{E}_i$ in kJ mol^{-1} were chosen as follows. For $NO_{1\times1}$, NO_{hex}, and NH_3 we use the rather crude assumption that the activation energy for surface diffusion often amounts to about 20% of the bond strength of the adsorbate-metal bond. Using the values $E_1 = 37$, $E_4 = 28.5$, $E_5 = 18$ kcal mol^{-1} from table 2 (page 19), this yields $\tilde{E}_{\mathrm{NO}}^{1\times1} = 31$, $\tilde{E}_{\mathrm{NO}}^{\mathrm{hex}} = 22$, $\tilde{E}_{\mathrm{NH_3}} = 15$ kJ mol^{-1}. For diffusion of N and H we may use the experimental values [2] $\tilde{E}_{\mathrm{N}} = 87$ and $\tilde{E}_{\mathrm{H}} = 18$ kJ mol^{-1} from the chemically similar systems W(110)/N and Rh(111)/H. In the temperature range considered here, N, as well as O with $\tilde{E}_{\mathrm{O}} \approx 150$, cf.[2], may then be considered to be immobile, hence we set $D_{\mathrm{N}} = D_{\mathrm{O}} = 0$. Moreover, in our problem we have $D_3 = D_{1\times1} = 0$ since the $1\times1 \leftrightarrow$ hex transition is not

process	parameter	$\tilde{E}$ (kJ mol^{-1})	value at 420K (cm^2 s^{-1})
NO–diffusion (1×1)	$D_1 = D_{\rm NO}^{1\times1}$	28	3.3×10^{-7}
NO–diffusion (hex)	$D_2 = D_{\rm NO}^{\rm hex}$	22	1.8×10^{-6}
N.A.	$D_3 = 0$	N.A	always=0
NH_3–diffusion	$D_4 = D_{\rm NH_3}$	15	1.4×10^{-5}
O–diffusion	$D_5 = D_{\rm O}$	N.A.	always set to 0
N–diffusion	$D_6 = D_{\rm N}$	N.A.	always set to 0
H–diffusion	$D_7 = D_{\rm H}$	18	5.7×10^{-6}

N.A. means not applicable

Table 1: The standard diffusion energies (SDE) and constants

diffusive but encoded in the ODEs (1.1).

We remark again that these diffusion energies are rough estimates only. Moreover, more realistic models might need coverage–dependent diffusion energies, i.e. nonlinear diffusion $\mathrm{div}(M(t,X)\nabla X)$ (the data in [2] was given at 0.1 local coverage). In fact, there are nonlinear corrections (A.2) to the bonding energies E_1 and E_5, and the average E_1 along the periodic orbits is between 26.5 kJ mol^{-1} ($T = 410$) and 28.3 kJ mol^{-1} ($T = 430$). Thus, we take the freedom to change $\tilde{E}_{\rm NO}^{1\times1}$ from 31 kJ mol^{-1} to 28 kJ mol^{-1} in table 1, summarizing our data. Henceforth, this data will be called standard diffusion energies (SDE), and will be our starting point to study how changes in D_i can change the behavior of the system.

Note that these diffusion constants differ quite significantly in magnitude, which is why we call diffusion of $NO_{1\times1}$ and $NO_{\rm hex}$ relatively slow and that of H and NH_3 relatively fast. In this sense (strictly speaking for $D_{\rm NO}^{1\times1} = D_{\rm NO}^{\rm hex} = 0$) (1.2) is related to the model problem in [13] where a field of oscillators is coupled by diffusion through a passive medium. Previewing section 5, we remark that the "typical pattern size" l_p of SW for (1.2) with SDE at T=420 will be of the order of 0.01cm. Hence $\sqrt{D_{\rm NH_3}\tau}\approx3.7\times10^{-3}$cm and $\sqrt{D_{\rm H}\tau} \approx 2.4\times10^{-3}$cm, where $\tau = 1$s is our time–scale, are roughly of the magnitude as l_p and diffusions of $\theta_{\rm NO}^{\rm hex}$ and $\theta_{\rm N}^{1\times1}$ introduce a nonlocal but also nonglobal coupling, where local (global) coupling would correspond to $\sqrt{D_{\rm NH_3}\tau} \ll l_p$ ($\sqrt{D_{\rm NH_3}\tau} \gg l_p$). On the other hand, we will find phase waves for (1.2) for smaller $D_{\rm NH_3}, D_{\rm H}$, e.g., when $D_{\rm NH_3}$=$D_{\rm H} \approx 0.8\times10^{-6}$ cm^{2}s^{-1} ($\sqrt{D_{\rm NH_3}}$=$\sqrt{D_{\rm H}} \approx 0.9\times10^{-3}$ cm s^{-1}), that is, when we approach the local coupling regime.

Henceforth, T, $\tilde{E}_i$ and D_i will be given without units; it is understood that T is in Kelvin and that the diffusion energies are in kJ mol^{-1} and the diffusion constants in cm^2 s^{-1}.

4.2 Numerical method and system size

To discretize (1.1) we choose a system size L (in cm), and consider n oscillators $X(\cdot,i)$=$X(\cdot,x_i)$ at $x_i = i$dx, i=1, ..., n, dx = $L/(n-1)$, with periodic boundary conditions. The discretized

system is then solved using a second order split–step method: we choose an effective time step dt > 0, alternatingly integrate by dt the ODE–part using the linearly implicit solver `limex` [6, section 6.4] (available online at `www.zib.de/SciSoft/CodeLib/ivpode.en.html`) and the linear PDE–part $\frac{\mathrm{d}}{\mathrm{d}t}X = M\nabla^2 X$ using an implicit Fourier spectral method; this is followed by Richardson extrapolation in order to obtain a second order method and to have error and time step control. Convergence in dx was checked by reducing dx by a factor of two and comparison. In our simulations we use dx $= 0.0005$cm and the average effective time steps were about dt $= 0.001 \sim 0.01$ s (depending on T and the other parameters). Note that the implicit Fourier time-stepping for the diffusion is always stable, while `limex` already uses internal stepsize control. In fact, due to the rather small diffusion constants the stiffness in (1.2) coming from the ODE–part is as bad as that coming from diffusion. The ODEs can be integrated very efficiently using `limex`, and the difficulty here is the interplay between the surface explosion in the ODE and diffusion.

During the integrations we also monitored the various mass balance constraints; the simplest are $0 \le X_j(t,x) \le 1$ for all t, x, $j = 1, \ldots, 7$, but there are several more, e.g., $\theta^{1\times1}_{\mathrm{NO}} + \theta^{1\times1}_{\mathrm{NH_3}} + \theta^{1\times1}_{\mathrm{O}} + \theta^{1\times1}_{\mathrm{N}} + \theta^{1\times1}_{\mathrm{H}} \le \theta_{1\times1}$, for obvious reasons. For the ODE these conditions are always fulfilled, but due to diffusion we have to introduce an error tolerance for them in (1.2), which was chosen as $\delta = 10^{-4}$. This was only a problem for high temperatures: for $T \ge 426$ typical (nontrivial) solutions yield $\theta^{1\times1}_{\mathrm{O}}, \theta^{1\times1}_{\mathrm{H}} \le -\delta$ and the integrations were aborted.

The experimental data in [24] was reported for a sampled area of size about $1\mathrm{mm}^2$. Here, because we are in particular interested in SW and PC, we consider smaller samples (n=80, dx $= 0.0005$ cm, and hence L=0.0395 cm in most of the simulations). Using n=80 gives sufficiently many oscillators to show the mechanism and gives fast results with typically short transient behavior which hence can be suitably plotted. Hence we consider these small scale simulations a good starting point for a numerical exploration of the model, though the rather few oscillators together with the periodic boundary conditions do introduce constraints; see sections 5.3 and 5.4 for larger scale simulations and further discussion. On the other hand, periodic boundary conditions have numerical advantages, and the obtained patterns can be thought of clips from larger patterns. This is usually justified if the internal wavelength is much smaller than the whole (unclipped) domain.

4.3 Choice of initial conditions and method of presentation

The initial conditions (IC) for (1.2) were chosen as localized perturbations of the point $Z_0 = (0.03, 0.24, 0.22, 0.5\times10^{-6}, 0.01, 0.02)$ which is roughly near the end of segment 1 of the periodic orbit $\gamma(420)$, cf. fig.1. That means, we first assign $X(t = 0, x_i) = Z_0$ to all oscillators, then choose $k \in N$, $l \in \{0, \ldots, 7\}$ and $a \in \mathbb{R}$, and add a step of width $2k$ and

amplitude a to the lth component in the middle of the domain, i.e., we set

$$X_l(t{=}0, x_{\rm mid}{+}i{*}{\rm dx}) = z_l + a, \quad i = n/2{-}k, \ldots, n/2{+}k{-}1, \quad x_{\rm mid} = (n/2{-}1){\rm dx}. \tag{4.1}$$

Combinations of step-like perturbations in multiple components and at multiple x–positions were also used but yield no essential new results which however become more difficult to present.

It turns out that the BO solution $X_{\rm BO}$ is stable in the parameter regime given by table 1. Hence, in (4.1) we need sufficiently large k and/or a, depending on l, to push the system at least transiently away from $X_{\rm BO}$. As should be expected from the ODE reduction (1.3), the easiest way to perturb the system away from $X_{\rm BO}$ is to introduce perturbations in $\theta^{1\times1}_{\rm NO}, \theta^{\rm hex}_{\rm NO}$ or $\theta_{1\times1}$, i.e., to choose $l \in \{1,2,3\}$. Choosing $l \in \{4,5,6,7\}$ requires relatively large $|a|$, which tends to violate the mass constraints above. For the sake of brevity we restrict to perturbations in $\theta_{1\times1}$ ($l = 3$), fix $k = 4$, and vary a. Note that this way we add a perturbation to a non diffusive component and hence the system can only be driven away from from $X_{\rm BO}$ by coupling to the diffusive components.

We focus on plotting $\theta_{1\times1}(t,x)$ as the main diagnostic for (1.2). As explained in sec.2, $\theta_{1\times1}$ sets the timescale in the largest segment 1 of the ODE–orbits. Hence, for the reaction–diffusion problem we expect that for given $\theta_{1\times1}$ the remaining variables can roughly be read from fig.1, at least at values in segment 1 of the ODE–orbit. This turns out to be true for $\theta^{1\times1}_{\rm NO}, \theta^{\rm hex}_{\rm NO}, \theta^{1\times1}_{\rm O}, \theta^{1\times1}_{\rm N}$, and some special care is taken for $\theta^{1\times1}_{\rm NH_3}$ and $\theta^{1\times1}_{\rm H}$ due to their fast diffusion. Moreover, $\theta_{1\times1}$ gives easily comprehensible plots, which however will be complemented with additional diagnostics like the chemically important spatial averages $\langle\theta_{1\times1}\rangle$ and $\langle r_{\rm N_2}\rangle$, where, e.g, $\langle\theta_{1\times1}\rangle(t) = \frac{1}{n}\sum_{i=1}^{n}\theta_{1\times1}(i,t)$.

5 Simulations at $T = 420$

5.1 Standard diffusion energies

Figure 2 shows greyscale plots of our first simulation of the PDE (1.2). The parameters

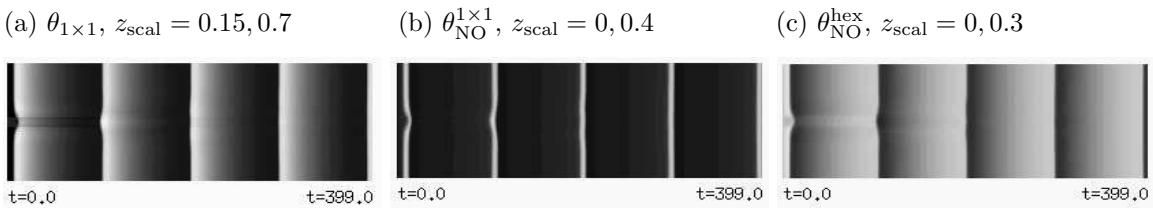

Figure 2: Reaction–diffusion problem (1.2) at T=420, standard diffusion energies (SDE) from table 1, dx=0.0005cm, n=80 (L=0.0395cm), IC according to (4.1) with $a = 0.06$: fast synchronization of the whole surface; $z_{\rm scal}$ as noted.

are $T = 420$, SDE (table 1), dx = 0.0005cm, $n = 80$ (hence system size $L = 0.0395$cm),

and IC according to (4.1) with $a = 0.06$. This yields the BO solution $X_{\rm BO}$. Additional to $\theta_{1\times1}$ we also plot $\theta^{1\times1}_{\rm NO}, \theta^{\rm hex}_{\rm NO}$. The greyscales are linear interpolations between $z_{\rm min}$=black and $z_{\rm max}$=white. The effect of the diffusive coupling is to even out the small phase perturbation introduced by the (small) perturbation of $\theta_{1\times1}$ at $t = 0$. In particular, the convergence to $X_{\rm BO}$ is very rapid (only 3 ODE cycles), in accordance with the theory outlined in sec.3.

However, for slightly larger initial perturbation $a = 0.1$ ($a = 0.07$ is sufficient) the solution does not relax to $X_{\rm BO}$ but to a SW solution $X_{\rm SW}$, see fig.3. Here, the larger value of $\theta_{1\times1}$ at $t = 0, x = x_{\rm mid}$ inhibits the NO adsorption; this then inhibits the $1\times1\leftrightarrow$ hex phase transition at $x_{\rm mid}$ until $\theta_{1\times1}$ has sufficiently decayed at $t \approx 60$, and eventually leads to the evolution of a regular grid of phase–clusters. The surface organizes into areas where it is in a periodic

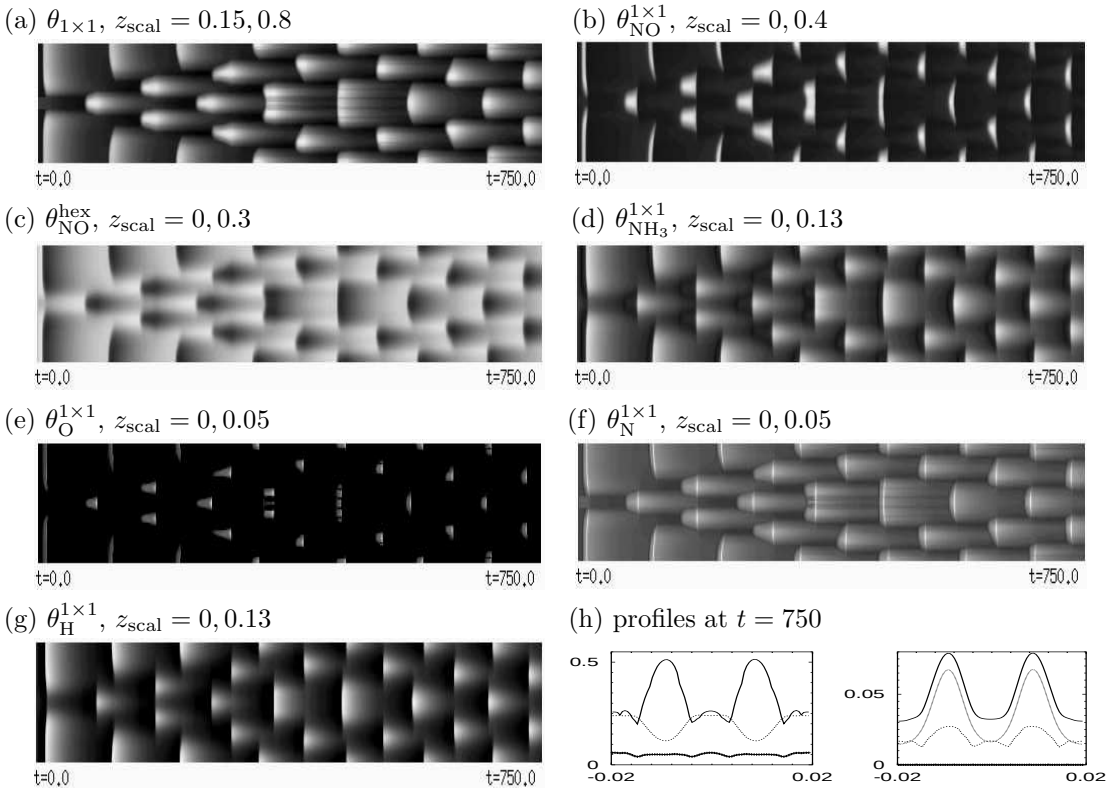

Figure 3: Same parameters as in fig.2 but with initial perturbation of amplitude $a = 0.1$; in (h) the left panel shows (top down, i.e., decreasing in magnitude) $\theta_{1\times1}, \theta^{\rm hex}_{\rm NO}, \theta^{1\times1}_{\rm NO}$ and the right panel $\theta^{1\times1}_{\rm NH_3}, \theta^{1\times1}_{\rm H}, \theta^{1\times1}_{\rm N}$ and $\theta^{1\times1}_{\rm O} (\approx 10^{-6})$.

orbit near $\gamma(420)$, but the phase of this periodic orbit changes in a regular fashion from one area to the next. Here we remark again that by definition the solution in fig.3 is a SW, since it has an intrinsic spatial wavelength (see sec.5.3), but that nevertheless for simplicity we call areas of equal phase clusters.

The phase–shift is exactly π, i.e., half a period, cf. sec.3. The process is almost complete at $t \approx 750$, and for $t > 1000$ we have a perfectly periodic solution. There is a phase balancing,

i.e., the area of the surface in each phase is equal. From $\theta_{\rm NO}^{1\times1}$, $\theta_{\rm NO}^{\rm hex}$ in (b),(c) we see the inhibition of NO adsorption at initial time, and how the evolution towards the SW looks in these variables. In contrast to (a–c) where we have rather sharp interfaces between the clusters, these are smoothed out for $\theta_{\rm NH_3}^{1\times1}, \theta_{\rm H}^{1\times1}$ in (d),(g) due to the fast diffusion of these variables. The non diffusive $\theta_{\rm O}^{1\times1}, \theta_{\rm N}^{1\times1}$ in (e,f) have sharp interfaces again. Finally in (h) we plot the solution at $t = 750$. The right panel shows again that $\theta_{\rm NH_3}^{1\times1}, \theta_{\rm H}^{1\times1}$ are smoother than the other variables.

In fig.4(a) we show $\theta_{1\times1}(t,i)$, $i = 1, 8, 12$, and in (b),(c) the averages $\langle\theta_{1\times1}\rangle, \langle r_{\rm N_2}\rangle$ together with the respective values $\theta_{1\times1}^{\rm ODE}, r_{\rm N_2}^{\rm ODE}$ from the ODE orbit. The evolution towards the SW

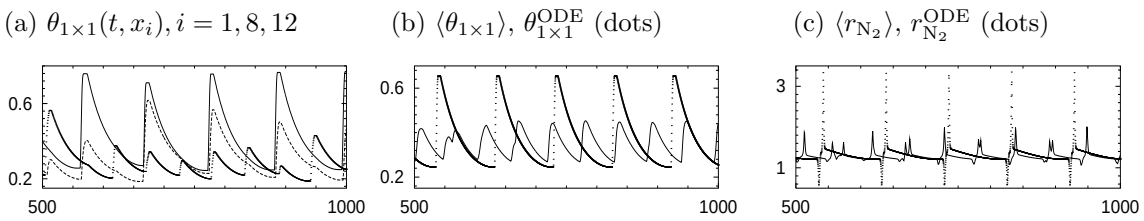

Figure 4: Time series for fig.3, with comparison to ODE solution; (a) $\theta_{1\times1}(t,x_1)$, $\theta_{1\times1}(t,x_8)$ (dashed) and $\theta_{1\times1}(t,x_{12})$(dots).

can be well observed in $\langle\theta_{1\times1}\rangle$ at about $t = 600$, where $\langle\theta_{1\times1}\rangle$ starts to oscillate in half of the period of the individual oscillators. This might explain why (after a temperature translation) the periods measured experimentally are about half as long as the periods in (1.1) [14, fig.7]. The period of the oscillations in the PDE is somewhat longer than in the ODE, i.e., the SW introduces a small time lag for each individual oscillator. Finally, the sharp peaks in, e.g., $r_{\rm N_2}$ are smoothed out in $\langle r_{\rm N_2}\rangle$ which also fits better with experimental data [14, fig.3].

The "phase–jumps" from one cluster to the next, together with the needed significant decrease of amplitude (here, e.g., $\theta_{1\times1}(1)$ has higher amplitude than $\theta_{1\times1}(8)$ and $\theta_{1\times1}(12)$, which "see" two clusters) from the center of the cluster to its boundaries, have the important consequence that this situation can never be described by a phase–diffusion equation (which requires smooth changes in phase).

5.2 Dependence on the diffusion constants

Next we study how $X_{\rm SW}$ depends on the diffusion constants (energies) and show a transition between SW and PC. We start with the rather sensitive dependence on $\tilde{E}_{\rm NO}^{1\times1}$ and $\tilde{E}_{\rm NO}^{\rm hex}$. In fig.5 we only show two simulations. In (a) we set $\tilde{E}_{\rm NO}^{1\times1} = 30$ ($D_{\rm NO}^{1\times1} = 1.9 \times 10^{-7}$), remaining parameters and IC as in fig.3, and obtain a SW with 6 clusters, in contrast to the SW with 4 clusters in fig.3 with $\tilde{E}_{\rm NO}^{1\times1} = 28$. Here, as always, all diffusion energies are in $\mathrm{kJ\,mol^{-1}}$ and all diffusion constants in $\mathrm{cm^2\,s^{-1}}$. On the other hand, in (b) we set $\tilde{E}_{\rm NO}^{1\times1} = 28$ again but $\tilde{E}_{\rm NO}^{\rm hex} = 24$ ($D_{\rm NO}^{\rm hex} = 1.0{\times}10^{-6}$), which yields only 2 clusters; for $t > 750$ the system evolves further to 2 clusters of equal size, hence fulfilling the principle of phase balance. In fact,

(a) $(\tilde{E}_{\rm NO}^{1\times1}, \tilde{E}_{\rm NO}^{\rm hex}) = (30, 22)$, 6 clusters.

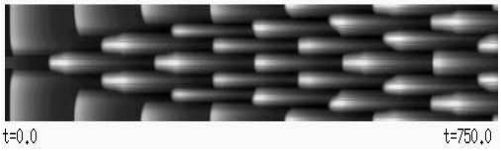

(b) $(\tilde{E}_{\rm NO}^{1\times1}, \tilde{E}_{\rm NO}^{\rm hex}) = (28, 24)$, 2 clusters.

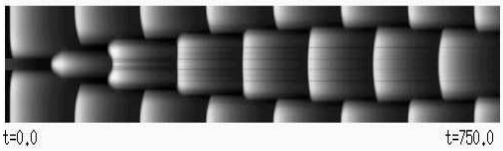

Figure 5: Influence of $\tilde{E}_{\rm NO}^{1\times1}$ and $\tilde{E}_{\rm NO}^{\rm hex}$ on cluster size; $\theta_{1\times1}$, $z_{\rm scal} = 0.13, 0.9$ (a), $z_{\rm scal} = 0.18, 0.73$ (b); IC and remaining parameters from fig.3.

previewing sec.5.3 we remark that this is a PC solution since the cluster size is not intrinsic: using larger scale simulations we find that the system again evolves to only 2 clusters.

The effect exemplified in fig.5 has been confirmed by several further simulations, using different initial conditions, system sizes, and rather small changes in $\tilde{E}_{\rm NO}^{1\times1}, \tilde{E}_{\rm NO}^{\rm hex}$: for SW, larger $D_{\rm NO}^{\rm hex}$ gives smaller clusters, i.e., a smaller spatial wavelength, while larger $D_{\rm NO}^{1\times1}$ gives larger clusters or may induce a transition from SW to PC. Hence it is natural to call diffusion of $\theta_{\rm NO}^{1\times1}$ *stabilizing* and diffusion of $\theta_{\rm NO}^{\rm hex}$ *destabilizing*. In fact, increasing (decreasing) $D_{\rm NO}^{1\times1}$ ($D_{\rm NO}^{\rm hex}$) can switch from SW or PC to BO, and decreasing (increasing) $D_{\rm NO}^{1\times1}$ ($D_{\rm NO}^{\rm hex}$) acts the other way round. In particular, it is possible to go from fully developed SW or PC to BO by increasing (decreasing) $D_{\rm NO}^{1\times1}$ ($D_{\rm NO}^{\rm hex}$) by less than ±4 during the simulation. Finally we remark that, as might be expected, for large $\tilde{E}_{\rm NO}^{1\times1}$ (i.e. for small stabilization by diffusion of $\theta_{\rm NO}^{1\times1}$) or small $D_{\rm NO}^{\rm hex}$ (large destabilization by diffusion of $\theta_{\rm NO}^{\rm hex}$) there exists an irregular regime where (small) clusters appear and disappear in a turbulent way. This regime, however, we leave for future work.

The dependence on $\tilde{E}_{\rm NH_3}$ and $\tilde{E}_{\rm H}$ is somewhat less sensitive than that on $\tilde{E}_{\rm NO}^{1\times1}, \tilde{E}_{\rm NO}^{\rm hex}$. In a series of simulations with (mainly) lower diffusions of H and NH_3 we found 2 effects. First, near the parameter regime from table 1, decreasing $D_{\rm NH_3}, D_{\rm H}$ increases the cluster size and may induce a transition from SW to PC. Secondly, decreasing $D_{\rm NH_3}, D_{\rm H}$ also destabilizes $X_{\rm BO}$ towards nontrivial solutions.

This is illustrated in fig.6, where we consider the joint effect of setting $\tilde{E}_{\rm NH_3}$=$\tilde{E}_{\rm H}$=25 ($D_{\rm NH_3}$=$D_{\rm H}$=7.8×10^{-7}), remaining parameters as in fig.3. For initial perturbations of amplitude $a = 0.1$ in (a) we obtain a PC solution (since we also obtain only 2 clusters for larger domains), in contrast to the SW with 4 clusters in fig.3. Moreover, a further bifurcation has occurred, and unlike in fig.5(b) the system does not eventually relax to 2 clusters of equal size. Instead, we have oscillating clusters (OPC): the cluster boundaries oscillate with a period much longer than the ODE period, as illustrated in fig.6(b), and this behavior goes on forever. For initial perturbations with $a = 0.05$ in (c) there is no clustering. However the system does not relax to $X_{\rm BO}$ as in fig.2 either, but a nontrivial phase wave evolves. For $t > 750$ the system is periodic with the wave profile that can be seen near $t = 700$; (d) shows $\theta_{\rm NO}^{1\times1}$ from (c). Hence, while in fig.3 we have competition between BO and SW (depending on the IC), here we have competition of PW and OPC. It is tempting to speculate that these

(a) $a = 0.1$, $\theta_{1\times1}$, 2 clusters (PC),

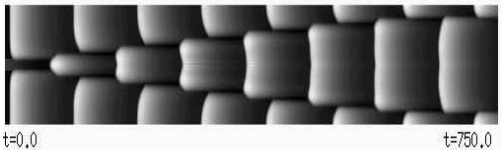

(b) with oscillating boundaries

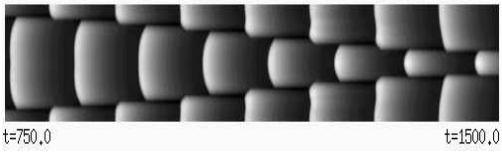

(c) $a = 0.05$, phase wave (PW), $\theta_{1\times1}$

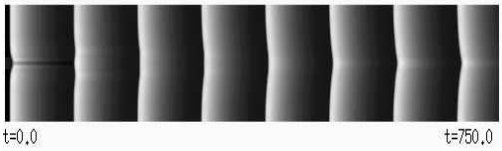

(d) $\theta_{\mathrm{NO}}^{1\times1}$ from (c).

Figure 6: $\tilde{E}_{\mathrm{NH_3}}$=$\tilde{E}_{\mathrm{H}}$=25, $\theta_{1\times1}$, remaining parameters from fig.3, z_{scal}=0.18, 0.73 (a,b), z_{scal}=0.2, 0.7 (c), z_{scal}=0, 0.4 (d)

phenomena are related.

As for the dependence on $\tilde{E}_{\mathrm{NO}}^{1\times1}, \tilde{E}_{\mathrm{NO}}^{\mathrm{hex}}$, these effects have been confirmed in a series of further simulations using different initial conditions, different values for $\tilde{E}_{\mathrm{NO}}^{1\times1}, \tilde{E}_{\mathrm{NO}}^{\mathrm{hex}}$, and moreover, using larger scale simulations. The effect of (artificially) setting $D_{\mathrm{NH_3}} = D_{\mathrm{H}} = 0$ will be studied in sec.5.4.

5.3 The distinction between SW and PC

To illustrate and support our distinction between SW and PC we show the results of repeating the simulations from fig.3 and fig.5(b) for a domain twice as large, i.e., $n = 160$. For SDE in

(a) $\theta_{1\times1}$, SDE, $z_{\mathrm{scal}} = 0.15, 0.8$

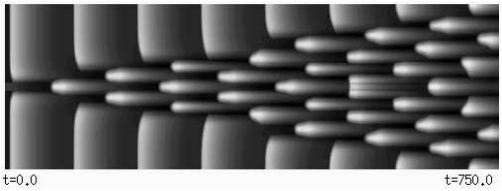

(b) large time for (a), SW with 8 clusters

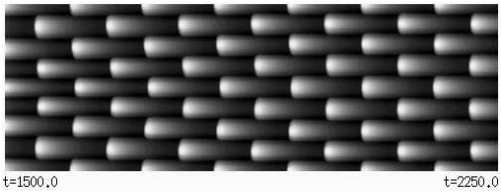

(c) $(\tilde{E}_{\mathrm{NO}}^{1\times1}, \tilde{E}_{\mathrm{NO}}^{\mathrm{hex}})$=(28, 24), $\theta_{1\times1}$, z_{scal}=0.18, 0.73

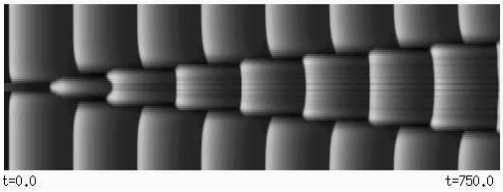

(d) large time for (c), PC

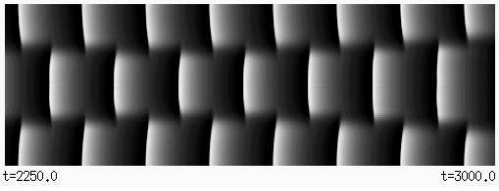

Figure 7: System size n=160, L=0.0795 cm, $T = 420$, initial conditions from (4.1) with $a = 0.1$; SDE in (a), $(\tilde{E}_{\mathrm{NO}}^{1\times1}, \tilde{E}_{\mathrm{NO}}^{\mathrm{hex}})$=(28, 24) in (b).

fig.7(a,b) we see that (after a rather long transient) the system relaxes to 8 clusters. Hence,

here the cluster–size is independent of n and the solution is a SW. The same happens, e.g., for $(\tilde{E}_{\rm NO}^{1\times1}, \tilde{E}_{\rm NO}^{\rm hex}) = (30, 22)$ (SW with 12 clusters in accordance with 6 clusters in fig.5(a)).

On the other hand, for $(\tilde{E}_{\rm NO}^{1\times1}, \tilde{E}_{\rm NO}^{\rm hex}) = (28, 24)$ the system needs a very long transient $t \approx 4000$ to relax to 2 clusters as in fig.5(b). Hence, here the cluster size is *not* intrinsic and the solutions in fig.5(b) and fig.7(c,d) are PC. Similarly, it can be checked that also on a larger domain the solution from fig.6(a,b) yields an OPC. Therefore, in theses regimes the periodic boundary conditions and the system size do add significant constraints. These will be even more important in the PW regime studied in sec.5.4.

5.4 Phase waves for vanishing diffusion of NH_3 and H

In fig.6(c,d) we found phase waves for relatively small diffusion of NH_3 and H. Here we consider the extreme case of $D_{\rm NH_3} = D_{\rm H} = 0$, in particular because of the relation to the naively reduced model (1.4). In order to minimize the effects of the periodic boundary conditions we run large scale simulations n=160 and also increase dx = 0.001cm, hence L=0.159cm. As usual, convergence in dx was checked. In fig.8 (a) with $(\tilde{E}_{\rm NO}^{1\times1}, \tilde{E}_{\rm NO}^{\rm hex})$=$(28, 22)$ the initial perturbation triggers two short counter propagating fronts. For large time we obtain a phase wave pattern with a periodic profile. Figure 8(b-c) shows that in a different parameter regime,

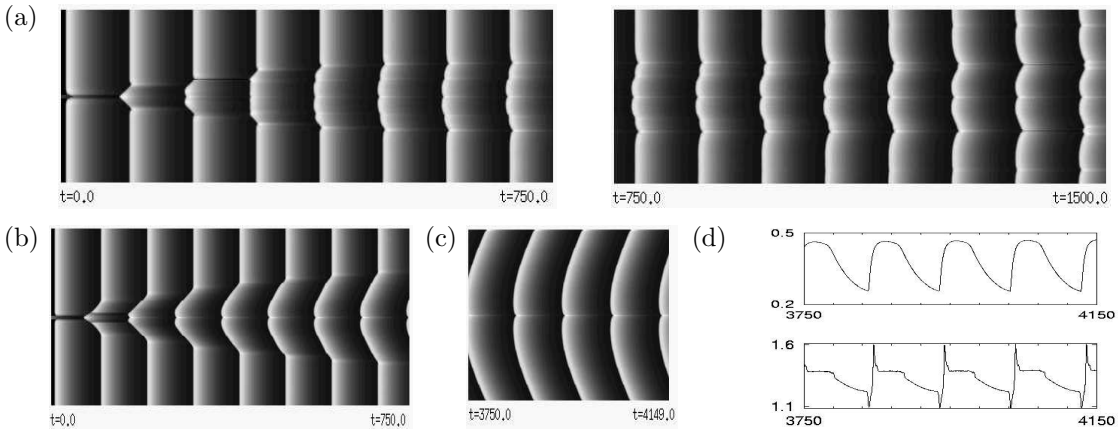

Figure 8: $D_{\rm NH_3} = D_{\rm H} = 0$, $n = 160$ points, greyscale plots of $\theta_{1\times1}$, $z_{\rm scal} = 0.15, 0.75$; $(\tilde{E}_{\rm NO}^{1\times1}, \tilde{E}_{\rm NO}^{\rm hex}) = (28, 22)$ in (a), $(\tilde{E}_{\rm NO}^{1\times1}, \tilde{E}_{\rm NO}^{\rm hex}) = (31, 29)$ in (b-d).

we can also produce longer fronts $(D_{\rm NO}^{1\times1} = 1.4 \times 10^{-7}, D_{\rm NO}^{\rm hex} = 2.5 \times 10^{-7})$. During a very long transient, the short and straight initial fronts (b) bend and eventually spread over the whole domain (c). Using even larger domains we find that for large time we always obtain solutions as in (c), which hence should be seen as phase fronts and not as phase waves with a periodic profile. Panel (d) shows $\langle\theta_{1\times1}\rangle$ (top) and $\langle r_{\rm N_2}\rangle$ (bottom) in this front regime.

In spite of extensive numerical simulations we could not find SW or PC for $D_{\rm NH_3}$=$D_{\rm H}$=0. The existence of PW in this regime does not contradict the results about non–existence of

PW from [9], outlined in sec.3, but rather confirms them. This theory holds for $0 < \mu \ll \varepsilon \ll 1$, and we expect $\mu \ll \varepsilon$ to be violated for the small coupling strength (via $D_{\mathrm{NO}}^{1\times1}, D_{\mathrm{NO}}^{\mathrm{hex}}$) considered in this section, or even for the situation in fig.6(c,d). The phase waves suggest a description by a phase diffusion equation, and the periodic PW in fig.8(a) is very likely due to a Turing bifurcation for this phase diffusion equation. However, we postpone this analysis to future work, see sec.7.

6 Temperature dependence

Roughly speaking, lowering temperature has a similar effect as decreasing (increasing) $D_{\mathrm{NO}}^{1\times1}$ ($D_{\mathrm{NO}}^{\mathrm{hex}}$), i.e., it becomes more difficult to obtain clustered solutions. In fig.9(a,b) with $T = 415$ and SDE from table 1 we need an initial perturbation of amplitude $a = 0.3$ in order to push the system away from X_{BO}. As in fig.5(b) and fig.7(c,d) the solution depends on the system size, i.e., also for larger domains we obtain 2 clusters, hence we have a PC solution. At $T = 410$ in fig.9(c) the system relaxes back to X_{BO} even for $a = 0.4$.

(a) $T = 415,\ a = 0.2$ (b) $T = 415,\ a = 0.3$, PC (c) $T = 410,\ a = 0.4$

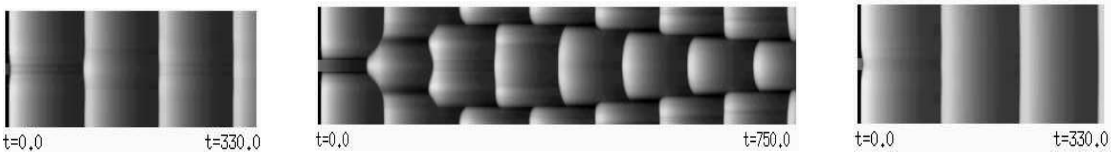

Figure 9: BO vs. PC at lower temperature; SDE, $\theta_{1\times1}$, $z_{\mathrm{scal}} = 0.3, 0.8$ in (a,b), $z_{\mathrm{scal}} = 0.4, 0.9$ in (c).

This behavior is somewhat counterintuitive since one might expect that less diffusion makes X_{BO} less stable and also leads to smaller clusters, hence SW rather than PC. On the other hand, we have two processes which might counteract. First, the periodic ODE orbit at T=415 has less sharp transitions and lower amplitude than at T=420. Second, as noted in sec.5.1, the diffusions of $\mathrm{NO}_{1\times1}$ (stabilizing), of $\mathrm{NO}_{\mathrm{hex}}$ (destabilizing) and NH_3, H (nonlocal coupling) play different roles; here all diffusion constant are lowered uniformly with T (though in a nonlinear way). Therefore we redid the simulations in fig.9(a,b) with T=415 but using the diffusion constants from T=420, which yields qualitatively the same results. This is a strong hint that the sharper transitions and the larger amplitudes in the ODE orbits at higher temperatures are important for both SW and PC, and, moreover, favor SW over PC.

For $\tilde{E}_{\mathrm{NH_3}} = \tilde{E}_{\mathrm{H}} = 25$, where at $T = 420$ we have competition between OPC and PW (fig.6), the latter become dominant at lower temperatures. At $T = 415$ we obtain PW for initial perturbations of amplitude $a = 0.2$, fig.10(a), while only for $a = 0.3$ we obtain OPC. At $T = 410$, only PW remain for these lower values of $\mathrm{NH_3}$ and H diffusion; see fig.10(b) with $a = 0.5$ for an example. As usual, these findings have been confirmed by several further simulations.

(a) $T = 415$, $a = 0.2$, $\theta_{1\times1}$, $z_{\rm scal} = 0.3, 0.8$ (b) $T = 410$, $a = 0.5$, $\theta_{1\times1}$, $z_{\rm scal} = 0.4, 0.9$

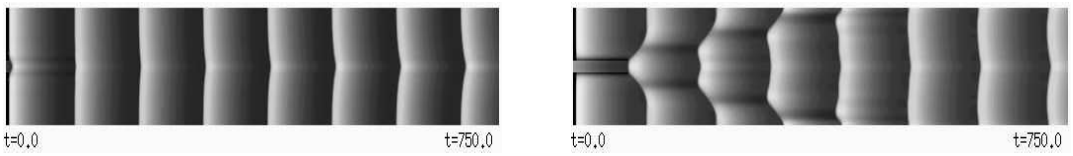

Figure 10: Dominance of PW at lower temperatures; $(\tilde{E}^{1\times1}_{\rm NO}, \tilde{E}^{\rm hex}_{\rm NO})$=(28, 22), $\tilde{E}_{\rm NH_3}$=$\tilde{E}_{\rm H}$=25.

Increasing temperature has the opposite effect. For instance, for $T = 423$ and SDE we obtain a SW with 4 clusters for initial perturbation of small amplitude $a = 0.02$. However, for higher T the numerics also become more and more difficult, i.e., dt has to be significantly decreased, and at $T = 426$ the system fails (for SDE) in the sense that $\theta^{1\times1}_{\rm O}$ and $\theta^{1\times1}_{\rm H}$ fall below the threshold $-\delta = -10^{-4}$ (cf. sec.4.2). Hence the integrations were aborted.

7 Discussion

Depending on temperature, the diffusion energies (constants) and the initial conditions we obtained bulk oscillations (BO), standing waves (SW), phase clusters (PC), oscillating phase clusters (OPC) or phase waves (PW) for (1.2). We found that diffusion of $\theta^{1\times1}_{\rm NO}$ (stabilizing BO) and $\theta^{\rm hex}_{\rm NO}$ (destabilizing BO) though small are the most sensitive parameters. The system is somewhat less sensitive with respect to $D_{\rm NH_3}, D_{\rm H}$; decreasing these may lead to SW with larger clusters or PC (with oscillating cluster boundaries) and also destabilizes BO towards PW. For small $D_{\rm NH_3}, D_{\rm H}$ no more SW or PC exist but only PW. In particular, the nonlocal coupling by the relatively fast diffusion of NH_3 and H is found to be a key ingredient for SW and PC: it replaces the global coupling through the gas phase in related models [1, 7, 8, 18].

Changes of temperature first of all affect the periodic ODE–orbits. At high temperatures they have a large amplitude and are highly anharmonic, which seems to be the second ingredient for SW and PC; at lower temperatures the orbits are less anharmonic and have a smaller amplitude which seems to favor BO or (for smaller $D_{\rm NH_3}, D_{\rm H}$) PW.

Essentially, we have picked points in parameter space (rather few) and given phenomenological descriptions. Mathematical explanations, relating the observed phenomena to the vector–field for the underlying ODE (1.1), seem rather difficult because of the complicated structure of (1.1). The results fit well with the mathematical theory for coupled relaxation oscillators [22, 9] outlined in sec.3. Hence, for a mathematical evaluation of, for instance, the different roles of $\tilde{E}^{1\times1}_{\rm NO}, \ldots, \tilde{E}_{\rm H}$ it looks promising to follow, e.g., [9] and calculate the function H in the pertinent generalization

$$\frac{\rm d}{{\rm d}t}\phi_i = H(\phi_{i-N}, \ldots, \phi_{i-1}, \phi_i, \phi_{i+1}, \ldots, \phi_{i+N}), \quad i = 1, \ldots, n, \tag{7.1}$$

of (3.2) and study how H and hence the system depends on $T, \tilde{E}^{1\times1}_{\rm NO}, \tilde{E}^{\rm hex}_{\rm NO}, \ldots$. Here ϕ_i is the phase of the ith oscillator and the nonlocal interactions $N > 1$ incorporate fast diffusion

of NH_3 and H. However, there are several difficulties in this approach. Technically, the derivation of (7.1) is impaired by the fact that the right hand side of (1.1) is only piecewise differentiable. More physically, in between the clusters in both SW and PC for (1.2) the oscillations are quite far from the periodic ODE orbits; see, e.g., fig.4(a). Hence it not clear whether (7.1) works in the SW/PC regime. On the other hand, it will be interesting to see whether a phase diffusion equation approach (continuum limit $n \to \infty$, dx $\to 0$ in (7.1), cf. sec.3) can be used to study, e.g., the instability of BO towards PW for lower diffusion of NH_3, H (fig.6(c,d), fig.8, fig.10).

Finally, it remains to study the 2–dimensional diffusion problem. In particular it will be interesting to see how that relates to experimental data [24, 14]. Also, although we showed that the role of global coupling through the gas phase in SW and PC is taken here by relatively fast diffusion of NH_3 and H, for comparison with experimental data it might be important to add a global coupling through the gas phase to (1.2).

These questions –including the approach (7.1) to (1.2)– will be subject to future work.

Acknowledgments. This work was partially carried out while the author was visiting INIFTA, La Plata, Argentina, and was partially supported by the DAAD project "Spatiotemporal chaos in heterogenous chemical reactions". The author thanks R. Imbihl, M. Bär, M. Rafti and E.E. Mola for stimulating discussions, and the INIFTA for the kind hospitality.

A The ODE

In order to make the paper sufficiently self contained, here we give the ODE (1.1); see [14, 23] for the chemical origins of the various terms and discussion:

$$\frac{\mathrm{d}}{\mathrm{d}t}\theta_{\mathrm{NO}}^{1\times1} = \mathrm{F}_{\mathrm{NO}}\mathrm{p}_{\mathrm{NO}}(\theta_{1\times1} - \theta_{\mathrm{NO}}^{1\times1} - 4\theta_{\mathrm{NH_3}}^{1\times1}) - k_1\theta_{\mathrm{NO}}^{1\times1} - k_2\frac{\theta_{\mathrm{NO}}^{1\times1}\theta_{\mathrm{empty}}^{1\times1}}{\theta_{1\times1}} + k_3\theta_{\mathrm{NO}}^{\mathrm{hex}}\theta_{1\times1} \ , \tag{A.1a}$$

$$\frac{\mathrm{d}}{\mathrm{d}t}\theta_{\mathrm{NO}}^{\mathrm{hex}} = \mathrm{F}_{\mathrm{NO}}\mathrm{p}_{\mathrm{NO}}(\theta_{\mathrm{hex}} - \theta_{\mathrm{NO}}^{\mathrm{hex}}) - k_3\theta_{\mathrm{NO}}^{\mathrm{hex}}\theta_{1\times1} - k_4\theta_{\mathrm{NO}}^{\mathrm{hex}} \ , \tag{A.1b}$$

$$\frac{\mathrm{d}}{\mathrm{d}t}\theta_{1\times1} = \begin{cases} (\frac{\mathrm{d}}{\mathrm{dt}}\theta_{\mathrm{NO}}^{1\times1})/\theta_{\mathrm{grow}}^{1\times1} & \text{if } \frac{\mathrm{d}}{\mathrm{dt}}\theta_{\mathrm{NO}}^{1\times1} > 0 \text{ and } \theta_{\mathrm{NO}}^{1\times1} \geq \theta_{\mathrm{grow}}^{1\times1}\theta_{1\times1} \text{ and } \theta_{1\times1} < 1 \ , \\ -k_{11}(\theta_{1\times1} - \theta_{\mathrm{def}}^{\mathrm{hex}})(1-c) & \text{if } \theta_{1\times1} > \theta_{\mathrm{def}}^{\mathrm{hex}} \text{ and c} < 1 \ , \\ 0 & \text{otherwise} \ , \end{cases} \tag{A.1c}$$

$$\begin{aligned}\frac{\mathrm{d}}{\mathrm{d}t}\theta_{\mathrm{NH_3}}^{1\times1} =& \mathrm{F}_{\mathrm{NH_3}}\mathrm{p}_{\mathrm{NH_3}}(\theta_{1\times1} - 3\theta_{\mathrm{NH_3}}^{1\times1} - 1.6\theta_{\mathrm{NO}}^{1\times1}) - k_5\theta_{\mathrm{NH_3}}^{1\times1} \\ & - k_6\frac{\theta_{\mathrm{NH_3}}^{1\times1}[\theta_{1\times1} - \theta_{\mathrm{H}}^{1\times1} - 2.5(\theta_{\mathrm{O}}^{1\times1} + \theta_{\mathrm{N}}^{1\times1})]}{\theta_{1\times1}} + k_7\frac{\theta_{\mathrm{N}}^{1\times1}\theta_{\mathrm{H}}^{1\times1}}{\theta_{1\times1}} \ ,\end{aligned} \tag{A.1d}$$

$$\frac{\mathrm{d}}{\mathrm{d}t}\theta_{\mathrm{O}}^{1\times1} = k_2\frac{\theta_{\mathrm{NO}}^{1\times1}\theta_{\mathrm{empty}}^{1\times1}}{\theta_{1\times1}} - k_8\frac{\theta_{\mathrm{O}}^{1\times1}\theta_{\mathrm{N}}^{1\times1}}{\theta_{1\times1}} \ , \tag{A.1e}$$

$$\frac{\mathrm{d}}{\mathrm{d}t}\theta_{\mathrm{N}}^{1\times1} = k_2\frac{\theta_{\mathrm{NO}}^{1\times1}\theta_{\mathrm{empty}}^{1\times1}}{\theta_{1\times1}} + k_6\frac{\theta_{\mathrm{NH_3}}^{1\times1}[\theta_{1\times1} - \theta_{\mathrm{H}}^{1\times1} - 2.5(\theta_{\mathrm{O}}^{1\times1} + \theta_{\mathrm{N}}^{1\times1})]}{\theta_{1\times1}} - k_7\frac{\theta_{\mathrm{N}}^{1\times1}\theta_{\mathrm{H}}^{1\times1}}{\theta_{1\times1}} - k_9\frac{(\theta_{\mathrm{N}}^{1\times1})^2}{\theta_{1\times1}}, \tag{A.1f}$$

$$\frac{\mathrm{d}}{\mathrm{d}t}\theta_{\mathrm{H}}^{1\times1} = \mathrm{F}_{\mathrm{H}_2}\mathrm{p}_{\mathrm{H}_2}\frac{[\theta_{1\times1}-\theta_{\mathrm{H}}^{1\times1}-2.5(\theta_{\mathrm{O}}^{1\times1}+\theta_{\mathrm{N}}^{1\times1})]^2}{\theta_{1\times1}} + 3\mathrm{k}_6\frac{\theta_{\mathrm{NH_3}}^{1\times1}[\theta_{1\times1}-\theta_{\mathrm{H}}^{1\times1}-2.5(\theta_{\mathrm{O}}^{1\times1}+\theta_{\mathrm{N}}^{1\times1})]}{\theta_{1\times1}}$$
$$- 3k_7\frac{\theta_{\mathrm{N}}^{1\times1}\theta_{\mathrm{H}}^{1\times1}}{\theta_{1\times1}} - 2k_8\frac{\theta_{\mathrm{O}}^{1\times1}\theta_{\mathrm{H}}^{1\times1}}{\theta_{1\times1}} - k_{10}\frac{(\theta_{\mathrm{H}}^{1\times1})^2}{\theta_{1\times1}}. \tag{A.1g}$$

The three conditions on the right hand side of (A.1c) have to be read top down and the first one fulfilled determines the right hand side. The rate constants $k_1, \ldots, k_{11}$ are determined by Arrhenius–law $k_i = \nu_i \mathrm{e}^{-E_i/RT}$, where the ν_i and most of the E_i are constants, given in table 2. For E_1 and E_5 coverage–dependent nonlinear corrections are used in the form

$$E_1 = E_1^0 - 24(\theta_{\mathrm{NO}}^{1\times1}/\theta_{1\times1})^2, \quad E_5 = E_5^0 - 30(\theta_{\mathrm{NH_3}}^{1\times1}/\theta_{1\times1})^2. \tag{A.2}$$

The auxiliary functions in (A.1) are given by

$$\theta_{\mathrm{empty}}^{1\times1} = \max\left[(\theta_{1\times1} - \frac{\theta_{\mathrm{NO}}^{1\times1}}{\theta_{\mathrm{NO}}^{\mathrm{inh}}} - \frac{\theta_{\mathrm{O}}^{1\times1}}{\theta_{\mathrm{O}}^{\mathrm{inh}}}), 0\right] + \max[(\theta_{\mathrm{def}}^{1\times1} - \theta_{\mathrm{O}}^{1\times1}), 0],$$
$$c = \left(\frac{\theta_{\mathrm{NO}}^{1\times1}}{\theta_{\mathrm{NO}}^{\mathrm{crit}}} + \frac{\theta_{\mathrm{O}}^{1\times1}}{\theta_{\mathrm{O}}^{\mathrm{crit}}}\right)/\theta_{1\times1}, \quad \theta_{1\times1} + \theta_{\mathrm{hex}} = 1, \quad \theta_{\mathrm{def}}^{1\times1} = \theta_{1\times1}\theta_{\mathrm{def}}, \quad \theta_{\mathrm{def}}^{\mathrm{hex}} = \theta_{\mathrm{hex}}\theta_{\mathrm{def}},$$

and the further parameters are given in table 3.

B Adiabatic reduction

For illustration, we eliminate $\theta_{\mathrm{N}}^{1\times1}$ from (1.2), i.e., we solve $f_5(X) = 0$ for $\theta_{\mathrm{N}}^{1\times1}$ and obtain

$$\theta_{\mathrm{N}}^{1\times1} = -\alpha_1 + \sqrt{\alpha_1^2/4 - \beta_1}, \qquad \begin{aligned}\alpha_1 &= (k_7\theta_{\mathrm{H}}^{1\times1} - k_2\theta_{\mathrm{empty}}^{1\times1} + 2.5k_6\theta_{\mathrm{NH_3}}^{1\times1}\theta_{\mathrm{O}}^{1\times1})/k_9,\\ \beta_1 &= k_6\theta_{\mathrm{NH_3}}^{1\times1}(\theta_{\mathrm{H}}^{1\times1} + 2.5\theta_{\mathrm{O}}^{1\times1} - \theta_{1\times1})/k_9,\end{aligned} \tag{B.1}$$

where we take the positive root for obvious reasons. This yields a system

$$\frac{\mathrm{d}}{\mathrm{d}t}\tilde{X} = \tilde{f}(\tilde{X}) + \tilde{M}\nabla^2\tilde{X}, \quad \tilde{X}=(\theta_{\mathrm{NO}}^{1\times1}, \theta_{\mathrm{NO}}^{\mathrm{hex}}, \theta_{1\times1}, \theta_{\mathrm{NH_3}}^{1\times1}, \theta_{\mathrm{O}}^{1\times1}, \theta_{\mathrm{H}}^{1\times1}), \quad \tilde{f}=(f_1, f_2, f_3, f_4, f_6, f_7), \tag{B.2}$$

where $\tilde{M} = \mathrm{diag}(D_{\mathrm{NO}}^{1\times1}, D_{\mathrm{NO}}^{\mathrm{hex}}, 0, 0, D_{\mathrm{N}}, D_{\mathrm{H}})$. Fig.11 compares the solutions of (B.2) and (1.2) at $t = 750$. The error even at this large lime is quite small, and in fact it is essentially due to a slightly longer period for the solutions of (B.2). As noted, $\theta_{\mathrm{O}}^{1\times1}$ (and in fact, all $\theta_{\mathrm{NH_3}}^{1\times1}, \theta_{\mathrm{O}}^{1\times1}, \theta_{\mathrm{N}}^{1\times1}, \theta_{\mathrm{H}}^{1\times1}$) too can

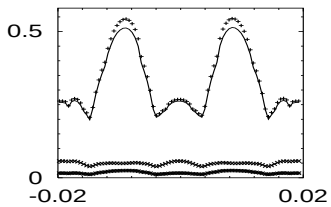

Figure 11: $\theta_{\mathrm{NO}}^{1\times1}$ ($\times$), $\theta_{1\times1}$ ($+$) and $\theta_{\mathrm{N}}^{1\times1}$ ($*$) at $t = 750$ for the solution of (B.2), initial conditions and remaining parameters from fig.3; the lines show the solution of (1.2).

be eliminated from (1.1), though it is algorithmically more complicated than the simple formula (B.1). However, in the SW and PC regimes elimination of $\theta_{\mathrm{O}}^{1\times1}$ yields a larger error, which must be attributed

to the fact that in these regimes many oscillators are far away from $\gamma(420)$ where elimination works best. Finally, in spite of the simple formula (B.1) the speedup in integration from (1.2) to (B.2) is very small. On the other hand, $\theta^{1\times1}_{NH_3}, \theta^{1\times1}_{H}$ due to their fast diffusion could only possibly be eliminated using a nonlocal reduction, which is of no computational benefit at all; see, e.g., [21, 13, 17] for such reductions in simpler model problems. For these reasons we consider adiabatic elimination, though it gives important insight into the ODE (1.1) [23], to be only of rather theoretical interest for the PDE (1.2) and ran our simulations for the full system (1.2).

reaction step	param.	ν_i (s^{-1})	E_i (kcal $\times$ mol^{-1})	value at 420K (s^{-1})
NO–desorption 1x1	k_1	1.7×10^{14}	37.0^a	9.7×10^{-6}
NO–dissociation 1x1	k_2	2.0×10^{15}	28.5	3.0
NO–trapping on 1x1	k_3	2.2×10^{4}	8.0	1.52
NO–desorption hex	k_4	4.0×10^{12}	26.0	0.12
NH_3–desorption 1x1	k_5	1.0×10^{9}	18.0^a	0.43
NH_3–dissociation 1x1	k_6	1.0×10^{15}	27.5	4.98
NH_3–formation 1x1	k_7	1.0×10^{10}	16.0	47.7
H_2O–formation 1x1	k_8	1.0×10^{13}	13.0	1.73×10^{6}
N_2–desorption 1x1	k_9	1.3×10^{12}	19.0	1.70×10^{2}
H_2–desorption 1x1	k_{10}	8.0×10^{12}	23.0	8.72
Transition 1x1→hex	k_{11}	2.5×10^{11}	25.0	2.48×10^{-2}

[a] for zero local coverage, see (A.2).

Table 2: Rate constants for the NO+NH3 reactions on Pt(100).

description	param.	value
NO–adsorption flux 1×1, hex	F_{NO}	$2.21 \times 10^5 (mbar^{-1}s^{-1})$
NH_3–adsorption flux 1×1	F_{NH_3}	$2.84 \times 10^5 (mbar^{-1}s^{-1})$
H_2–adsorption flux 1×1	F_{H_2}	$8.28 \times 10^5 (mbar^{-1}s^{-1})$
Inhibition coverage of NO for NO–dissociation	θ^{inh}_{NO}	0.61
Inhibition coverage of O for NO–dissociation	θ^{inh}_{O}	0.399
Critical coverage of NO for the 1×1→ hex phase transf.	θ^{crit}_{NO}	0.3
Critical coverage of NO for the 1×1→ hex phase transf.	θ^{crit}_{O}	0.4
Coverage for island growth in the hex→ 1×1 phase transf.	$\theta^{1\times1}_{grow}$	0.5
Amount of surface defects	θ_{def}	1.0×10^{-4}
partial pressures (tunable, but kept fixed here)	p_{NO}	1.1×10^{-6} mbar
	p_{NH_3}	4.7×10^{-6} mbar

Table 3: Temperature independent parameters.

References

[1] M. Bär, M. Hildebrand, M. Eiswirth, M. Falcke, H. Engel, and M. Neufeld. Chemical turbulence and standing waves in a surface reaction model: The influence of global coupling and wave instabilities. *Chaos*, 4:499–508, 1994.

[2] J.V. Barth. Transport of adsorbates at metal surfaces : From thermal migration to hot precursors. *Surf. Sci. Rep.*, 40(3–5):75–149, 2000.

[3] M. Bertram and A. S. Mikhailov. Pattern formation in a surface chemical reaction with global delayed feedback. *Phys. Rev. E*, 63:066102, 2001.

[4] M. Bertram and A. S. Mikhailov. Pattern formation on the edge of chaos: Experiments with CO oxidation on a Pt(110) surface under global delayed feedback. *Phys. Rev. E*, 67:036208, 2003.

[5] M. Bertram and A. S. Mikhailov. Pattern formation on the edge of chaos: Mathematical modeling of CO oxidation on a Pt(110) surface under global delayed feedback. *Phys. Rev. E*, 67:036207, 2003.

[6] P. Deuflhard and F. Bornemann. *Scientific computing with ordinary differential equations*, volume 42 of *Texts in Applied Mathematics*. Springer-Verlag, New York, 2002.

[7] M. Falcke and H. Engel. Pattern formation during the CO oxidation on Pt(110) surfaces under global coupling. *J. Chem. Phys.*, 101:6255–6263, 1994.

[8] M. Falcke, H. Engel, and M. Neufeld. Cluster formation, standing waves, and stripe patterns in oscillatory active media with local and global coupling. *Phys. Rev. E*, 52:763–771, 1995.

[9] E. M. Izhikevich. Phase equations for relaxation oscillators. *SIAM J. Appl. Math.*, 60(5):1789–1804, 2000.

[10] M. Kim, M. Bertram, M. Pollmann, A. von Oertzen, A. Mikhailov, H. H. Rotermund, and G. Ertl. Controlling chemical turbulence by global delayed feedback: Pattern formation in catalytic CO oxidation reaction on Pt(110). *Science*, 292:1357–1359, 2001.

[11] N. Kopell and G. B. Ermentrout. Mechanisms of phase-locking and frequency control in pairs of coupled neural oscillators. In *Handbook of dynamical systems, Vol. 2*, pages 3–54. North-Holland, Amsterdam, 2002.

[12] Y. Kuramoto. *Chemical oscillations, waves, and turbulence*, volume 19 of *Springer Series in Synergetics*. Springer-Verlag, Berlin, 1984.

[13] Y. Kuramoto, H. Nakao, and D. Battogtokh. Multi-scaled turbulence in large populations of oscillators in a diffusive medium. *Phys. A*, 288(1-4):244–264, 2000.

[14] S.J. Lombardo, T. Fink, and R. Imbihl. Simulations of the NO+NH_3 and NO+H_2 reactions on Pt(100): Steady state and oscillatory kinetics. *J. Chem. Phys*, 98(7):5526–5539, 1993.

[15] A. Mielke, G. Schneider, and H. Uecker. Stability and diffusive dynamics on extended domains. In *Ergodic theory, analysis, and efficient simulation of dynamical systems*, pages 563–583. Springer, Berlin, 2001.

[16] V. I. Nekorkin and M. G. Velarde. *Synergetic phenomena in active lattices – Patterns, waves, solitons, chaos*. Springer Series in Synergetics. Springer-Verlag, Berlin, 2002.

[17] E. M. Nicola, M. Or-Guil, W. Wolf, and M. Bär. Drifting pattern domains in a reaction-diffusion system with nonlocal coupling. *Phys. Rev. E*, 65:055101(R), 2002.

[18] A. v. Oertzen, H. H. Rotermund, A. S. Mikhailov, and G. Ertl. Standing wave patterns in the CO oxidation reaction on a Pt(110) surface: Experiments and modeling. *J. Phys. Chem. B*, 104(14):3155–3178, 2000.

[19] K.C. Rose, D. Battogtokh, A. Mikhailov, R. Imbihl, W. Engel, and A.M. Bradshaw. Cellular structures in catalytic reactions with global coupling. *Phys. Rev. Lett.*, 76:3582–3585, 1996.

[20] E.G. Seebauer and C.E. Allen. Estimating surface diffusion coefficients. *Progress in Surface Science*, 49:265–330, 1995.

[21] M. Sheintuch and O. Nekhamkina. Reaction-diffusion patterns on a disk or a square in a model with long range interaction. *J. Chem. Phys.*, 107:8165–8174, 1997.

[22] D. Somers and N. Kopell. Waves and synchrony in networks of oscillators of relaxation and non-relaxation type. *Phys. D*, 89(1-2):169–183, 1995.

[23] H. Uecker, R. Imbihl, M. Rafti, I.M. Iruzun, J. L. Vicente, and E.E. Mola. Adiabatic reduction and hysteresis of the LFI–model of NO+NH_3 on Pt(100). Accepted by *Chem. Phys. Let.*, 2003.

[24] G. Veser, F. Esch, and R. Imbihl. Regular and irregular spatial patterns in the catalytic reduction of NO with NH_3 on Pt(100). *Catalysis Letters*, 13:371–382, 1992.

[25] L. Yang, M. Dolnik, A. M. Zhabotinsky, and I. R. Epstein. Oscillatory clusters in a model of the photosensitive Belousov-Zhabotinsky reaction system with global feedback. *Phys. Rev. E*, 62:6414–6420, 2000.